Electric field–induced migration and intercellular stress alignment in a collective epithelial monolayer

Youngbin Cho, Minjeong Son, Hyuntae Jeong, and Jennifer H. Shin*
Department of Mechanical Engineering, Korea Advanced Institute of Science and Technology, Daejeon 34141, Republic of Korea

ABSTRACT **During wound healing, cells migrate with electrotactic bias as a collective entity. Unlike the case of the electric field (EF)-induced single-cell migration, the sensitivity of electrotactic response of the monolayer depends primarily on the integrity of the cell–cell junctions. Although there exist biochemical clues on how cells sense the EF, a well-defined physical portrait to illustrate how collective cells respond to directional EF remains elusive. Here, we developed an EF stimulating system integrated with a hydrogel-based traction measurement platform to quantify the EF-induced changes in cellular tractions, from which the complete in-plane intercellular stress tensor can be calculated. We chose immortalized human keratinocytes, HaCaT, as our model cells to investigate the role of EF in epithelial migration during wound healing. Immediately after the onset of EF (0.5 V/cm), the HaCaT monolayer migrated toward anode with ordered directedness and enhanced speed as early as 15 min. Cellular traction and intercellular stresses were gradually aligned perpendicular to the direction of the EF until 50 min. The EF-induced reorientation of physical stresses was then followed by the delayed cell-body reorientation in the direction perpendicular to the EF. Once the intercellular stresses were aligned, the reversal of the EF direction redirected the reversed migration of the cells without any apparent disruption of the intercellular stresses. The results suggest that the dislodging of the physical stress alignment along the adjacent cells should not be necessary for changing the direction of the monolayer migration.**

Monitoring Editor
Yu-Li Wang
Carnegie Mellon University

Received: Feb 7, 2018
Revised: Jun 14, 2018
Accepted: Jul 20, 2018

INTRODUCTION

Cells divide, differentiate, migrate or die in response to various physiological cues from the microenvironment. Among many factors that trigger cellular responses, the most prevalent cues are biochemical origins such as hormones, cytokines, growth factors, and other soluble molecules. In addition to biochemical factors, all cells produce membrane potential by segregating ions and charged molecules between plasma membranes to generate endogenous electric fields (EFs) from the early embryonic development (Funk, 2015). Bioelectricity, an endogenous electrical cue, can override most chemical gradients to promote electrotactic response, termed *electrotaxis*. Electrotaxis, the phenomenon by which cells migrate directionally to electrical stimulation, affects a number of physiological processes such as embryonic development, directing nerve cell growth, angiogenesis, cancer metastasis, and wound healing (McCaig *et al.*, 2004; Zhao, 2009; Cortese *et al.*, 2014). When exogenous EFs are applied to cells in culture to mimic the naturally occurring EF, they exert profound polarization effects, directing the cellular migration.

Cell migration is constitutive for multiple physiological settings to position the cells at appropriate places at a right timing during biological processes. For example, during the process of wound healing, the cells in our body must know not only when but, very importantly, in which direction to migrate, for effective healing of

This article was published online ahead of print in MBoC in Press (http://www.molbiolcell.org/cgi/doi/10.1091/mbc.E18-01-0077) on July 25, 2018.

The authors declare that they have no competing financial interest.

Author contributions: Y.C. and H.J. performed the experiment. Y.C., M.S., and J.H.S. analyzed and discussed the data. Y.C. and J.H.S. wrote the article.

*Address correspondence to: Jennifer H. Shin (j_shin@kaist.ac.kr).

Abbreviations used: dcEF, direct current electric field; EF, electric field; MSM, monolayer stress microscopy; PDMS, polydimethylsiloxane; TFM, traction force microscopy.

the wounded tissue. Numerous in vitro experiments confirmed the EF-induced directional migration in many cell types such as corneal epithelial cells (Zhao *et al.,* 1996, 1999, 2006; Song *et al.,* 2002), endothelial cells (Zhao *et al.,* 2003), keratocytes (Cooper and Schliwa, 1985; Sun *et al.,* 2013), keratinocytes (Nakajima *et al.,* 2015), and breast cancer cells (Mycielska and Djamgoz, 2004; Pu *et al.,* 2007). Both the speed and direction of electrotaxis are cell-type dependent. The typical range of physiologically relevant EF has been reported to be 0.1–10 V/cm. The physiological range of EF also induced significant morphological changes in many cell types, including endothelial cells (Zhao *et al.,* 2003), epithelial cells (Luther and Peng, 1983), neural crest cells (Cooper and Keller, 1984), and osteoblasts (Curtze *et al.,* 2004). The EF-induced reorientation was accompanied by the asymmetric redistribution of cytoskeletal structures such as actin stress fiber (Luther and Peng, 1983) and microtubule (Song *et al.,* 2002) as well as Golgi apparatus (Pu and Zhao, 2004). A number of researchers investigated the biomolecular intracellular signaling pathways to reveal how the cells sense and control the polarity in response to the directional electric cue at a single-cell level (McCaig and Zhao, 1997; Robinson, 1985). The intracellular "compass model" suggests a competition between the PI3K-dependent pathway at the front and the myosin-dependent pathway at the rear of the cell that determines the direction of single-cell migration by the active formation of lamellopodia in directional response to the applied EF (Sun *et al.,* 2013). The dcEF was shown to induce a polarized activation of several other signaling pathways such as phosphatase and tensin homologue (PTEN), epidermal growth factor (EGF) receptors, mitogen-activated protein kinase (MAPK), extracellular-signal-regulated kinase (ERK), and Src (Fang *et al.,* 1999; Zhao *et al.,* 1999, 2002, 2006; Pu *et al.,* 2007). Furthermore, with the advancement of techniques to visualize cellular traction, few researchers observed the surprisingly immediate response of cellular traction to the applied EF, which preceded the polarized rearrangement of the intracellular cytoskeleton in the cells cultured in low density (Harris *et al.,* 1990, Curtze *et al.,* 2004). These findings indicate that the physical traction may be the very early target of the EF-induced polarized signaling pathway during the electrotactic response.

The limitation of current knowledge is that the studies on the electrotactic response dealt with the cells that are in isolation without mature cell–cell adhesions. However, cellular motility in many physiological conditions concerns with the cluster of cells held by intimate cell–cell contacts. Especially during embryonic development and wound healing, a sheet of cells expands with electrotactic bias as a collective pack. Each cell in a cellular cluster is physically coupled to neighboring cells confining the cells in the monolayer while suppressing active lamellipodia. Consequently, the cell-cell interactions may induce the differential impact of the EFs on cells in the confluent monolayer, compared with the isolated cells. Recent studies demonstrated the different electrotactic response between single cells and a collective monolayer. Li *et al.* showed that the epithelial cells in a monolayer migrated far more efficiently with better directional persistence compared with those in isolation or smaller clusters (Li *et al.,* 2012). Interestingly, even within the monolayer, cells near the free edge, which show the distinct behavior compared with the cells in the bulk of the monolayer such as the emergence of leader cells with aligned actin stress fiber and weak E-cadherin, did not show the efficient electrotactic migration (Cohen *et al.,* 2014). Thus, one can speculate that the sensitivity of collective electrotactic response depends primarily on the integrity of the cell–cell junctions. While there exist biochemical clues on the EF-induced changes in the physical state of junctional proteins, the quantification of physical stresses that govern the EF-induced collective migration requires further investigation. More specifically, experimental observations on the EF-induced changes in the underlying tractions exerted by each cell on its substrate, and intercellular stresses exerted between immediate neighbors, have been a significant challenge. Consequently, a well-defined physical portrait to illustrate how collective cells respond to directional EF remains elusive.

In this work, we developed an EF stimulating system integrated with a hydrogel-based traction measurement platform to quantitatively measure the EF-induced changes in cellular tractions (Trepat *et al.,* 2009), from which the complete in-plane intercellular stress tensor can be obtained (Tambe *et al.,* 2011). Our observations showed initially randomly migrating HaCaT cells immediately responded and rapidly synchronized their migration toward the anode within 15–20 min after the onset of 0.5-V/cm EF stimulation. Cellular traction and intercellular stresses were gradually aligned perpendicularly to the direction of the EF until 50 min after stimulation. Furthermore, intercellular stress tensor perpendicular to the EF direction increased significantly while the stress tensor parallel to the EF direction decreased during the EF application. The overall magnitude of average intercellular stress maintained or slightly increased during the EF stimulation experiment. This reorientation of physical stresses under EF stimulation preceded the morphological reorientation perpendicular to the EF direction. Once the intercellular stresses were aligned, the disruption of the intercellular stress orientation was not necessary for changing the direction of monolayer migration during the reversal of EF direction.

RESULTS

Establishment of the EF–TFM (traction force microscopy) chamber

To quantify the immediate electrotactic response of a collective monolayer, we set up the EF stimulating system with the following specifications: 1) small size and transparency for real-time imaging on the microscope, 2) stable EF stimulation without fluctuations of temperature or pH, and 3) hydrogel-based traction measurement platform. For the size and transparency constraints, 76 × 52-mm-sized glass slides were used for the base part with a cover made of transparent polydimethylsiloxane (PDMS) membrane. To warrant stable EF stimulation without disturbing cell culture condition, we redesigned the EF stimulation platform by implementing several key geometrical features from the existing EF devices (Song *et al.,* 2007; Cohen *et al.,* 2014). Most importantly, the specific geometry and the medium reservoir height (Figure 1b) were carefully selected to minimize the undesirable effects of electrochemical byproducts and pH change while guaranteeing the linear EF lines (simulated by COMSOL Multiphysics Software in Figure 1c). Since the shallow clearance in the cell observation region yields high electrical resistance compared with the medium reservoir with higher depth, up to 60% of total voltage drop can be concentrated at the cell observation region (Figure 1d) (Cohen *et al.,* 2014). Also, a sufficient volume of medium in the chamber reservoir helped to maintain a stable pH and temperature within the chamber (Song *et al.*, 2007). Finally, the most critical feature of our device is the hydrogel-based traction measurement platform inside the EF stimulation system. To measure the cellular forces, we cultured the HaCaT cell monolayer on a fluorescence-bead-embedded polyacrylamide (PA) gel within the cell observation region (Figure 1b).

A glass slide and the first PDMS membrane with the pattern were first treated with O_2 plasma for the permanent bonding between

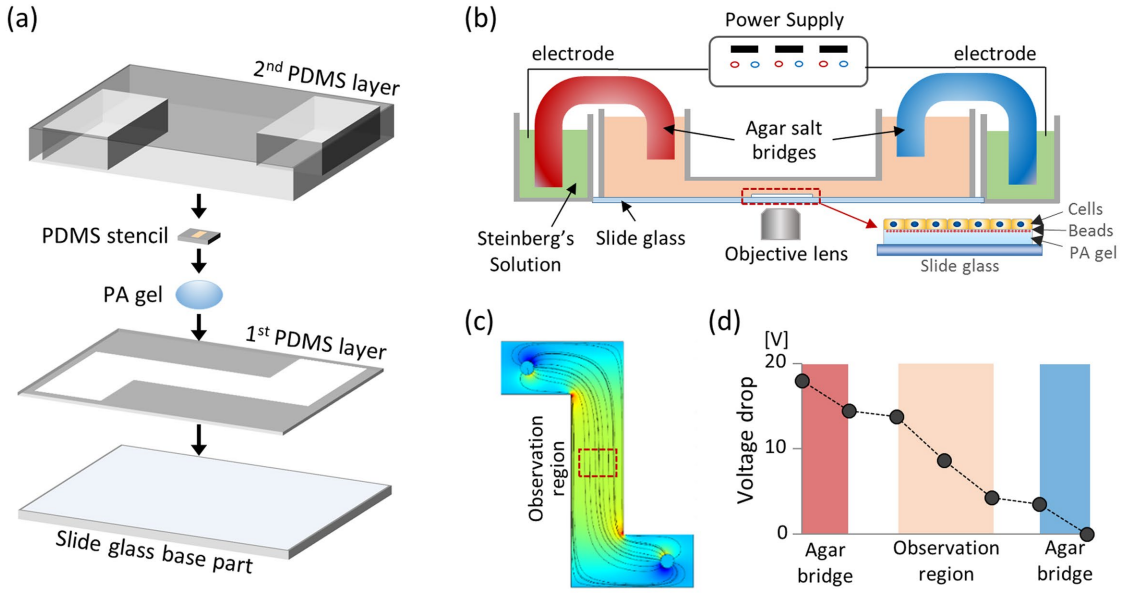

FIGURE 1: Establishment of EF stimulating chamber implemented with force measurement system. (a) Schematics of the chamber components and fabrication process. Polyacrylamide gel is embedded in the chamber for the force measurement. (b) Schematics of the experimental set-up for EF stimulation. Chamber is connected to the power supply through agar bridge and Steinberg's solution. Red dotted box in the middle of the chamber indicates the observation region for imaging. In the observation region, fluorescent bead–embedded PA gel is fabricated on the slide-glass surface. HaCaT monolayer was cultured on the PA gel to measure the traction force during the EF stimulation. (c) COMSOL simulation of the linear EF line at the cell observing area. (d) Experimental measurement of the voltage drop within the chamber. Owing to the high electrical resistance, up to 60% of total voltage drop was concentrated at the cell observation region (blue shaded region), indicating the enhancement of the voltage drop efficiency of the chamber.

two layers. After bonding two layers, the glass surface at the center of the observation region was pretreated with silane for the stable linkage between the glass and PA gel. Then, 10 µl of PA gel (3 kPa; 5.5% acrylamide, 0.09% bisacrylamide, 0.5% ammonium persulfate) mixed with 0.5-µm-diameter fluorescent beads was polymerized by pressing the 12-mm-diameter cover glass on the PA gel drop. During the polymerization of PA gel, the whole base part was centrifuged upside down for 15 min at 1000 rpm to pull up the beads to the surface of the gel. After polymerization, the surface of the PA gel was functionalized by Sulfo-SANPAH and then coated with 10 µg/ml collagen I for the cell attachment. To culture the HaCaT cells as a confluent monolayer slab, we prepared 250-µm-thick PDMS stencil with 1.8 mm^2-sized rounded rectangular patterns and gently pressed the stencil down on the gel surface. HaCaT cells were seeded within the PDMS stencil and incubated for 12 h to establish the confluent monolayer with mature cell–cell junctions. Before the start of the experiment, we peeled off the PDMS stencil to prevent the distortion of the EF near the cell monolayer. We then finalized the assembly of the chamber by placing a 6-mm-thick second PDMS layer, pretreated with O_2 plasma, onto the first PDMS membrane to seal the observation region. Agar bridges were placed between the reservoirs and the Steinberg's solutions with an Ag/AgCl electrode connected to the voltage controlled power source.

Immediate electrotaxis of collective epithelial monolayer in the direction of EF

In the absence of EF, HaCaT cells within the confluent monolayer migrated in random directions (Figure 2a). At the onset of 0.5 V/cm direct current EF (dcEF), the cells began to migrate toward the anode (upper direction in Figure 2, b–e). The anodal migration response was so rapid that the directed migration became predominant through the monolayer as early as 10 min after the onset of EF application. Continued exposure to the 0.5 V/cm EF for 30 min, the cell migration became almost completely ordered in the direction parallel to the EF with the directedness value of 0.97 where the directedness value of 1 indicates a perfect migratory alignment with the direction of the EF (Figure 2f; see *Materials and Methods* for details on the directedness). As such, the parallel component of the migration velocity ($V_{||}$) of the collective cells was greatly enhanced by approximately fourfold compared with the case without EF application. However, the perpendicular component of the velocity did not show any significant change (Figure 2g).

Perpendicular reorientation of cell body to the EF direction lags electrotactic migration

After the onset of DC EF, initially randomly oriented HaCaT cells gradually changed their orientation in the direction perpendicular to the EF (Figure 3, a, c–f). We compared the time-course electrotactic response of cell migration and cell-body reorientation using the rose plot at discrete time points of pre-EF, and 30, 50, 100 min after 0.5 V/cm dcEF application (Figure 3, b and g–j). While the anodal electrotactic migration response was immediate, the cellular reorientation happened gradually over 100 min. We took the absolute values for both velocity and cell-body orientations to plot the data within 0°–90° range. The cellular velocities were calculated by the PIV analysis, and the changes in the cell-body orientation were obtained by the ellipsoidal fit using the ImageJ (see *Materials and Methods* and Supplemental Figure S1). The red bars depict the velocity orientation, and the blue bars represent the cell-body orientation. Before the EF stimulation, the velocity and cell-body orientation were both

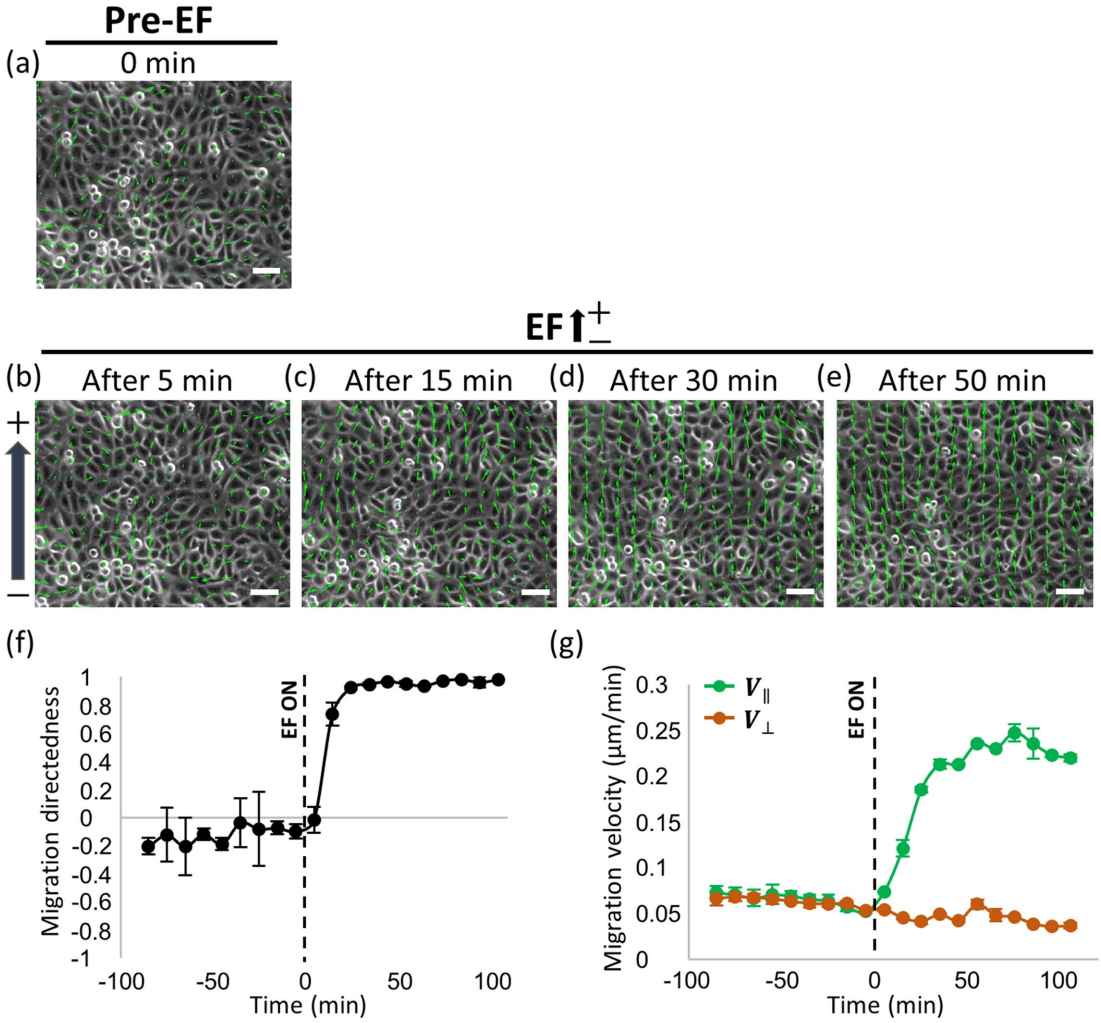

FIGURE 2: Immediate electrotactic migration in a collective monolayer. (a) Migration of HaCaT monolayer in the random direction at the pre-EF condition. (b–e) Time-course alignment of migration of HaCaT monolayer with the onset of EF stimulation. (b) Five minutes after start of EF, the monolayer still migrated in the random direction. (c) Within 15 min, the monolayer initiated the anodal migration. (d, e) With time, migration of overall monolayer aligned toward the anode. (f) Average migration directedness and (g) average migration velocity of HaCaT monolayer over time. Data are presented in 10-min intervals. Dashed lines indicate the time point of EF initiation. Data are presented as mean ± SD (n = 3 independent monolayers). Scale bars, 50 μm.

randomly distributed (Figure 3b). With the initiation of EF stimulation, the cellular velocities were biased early in the direction parallel to the EF within 30 min (Figure 3g). However, the cell body showed the tendency of perpendicular reorientation from 70 min after the EF stimulation (Figure 3i) and became apparent by 100 min (Figure 3j). Our data suggest that in HaCaT monolayer, the collective cellular electrotactic migration happens immediately after the onset of the EF, without having to require cellular reorientation or cytoskeletal rearrangement. Cell-body orientation, in fact, seems to follow the electrotactic migratory response with a time delay. This time delay may be due to the inherent property of the confluent monolayer where the neighboring cells are tightly bound to one another, hindering the morphological degree of freedom.

EF reorients cellular traction forces and intercellular stresses

When the cells migrate as a collective in a monolayer, cells generate both traction forces and intercellular stresses through the cell–substrate adhesions and cell–cell adhesions, respectively (Trepat *et al.*, 2009; Maruthamuthu *et al.*, 2011; Tambe *et al.*, 2011). Cells communicate intimately with the surroundings and neighboring cells through these cellular junctions (Gomez *et al.*, 2011). Both junction types are associated tightly with various structural molecules and cytoskeletal networks intracellularly (Vasioukhin *et al.*, 2000; le Duc *et al.*, 2010; Jang *et al.*, 2017). Cohen *et al.* (2014) reported a detailed portrait of the electrotactic migratory response of collective Madin–Darby canine kidney (MDCK) cells. Motivated by these findings, we became curious about the physical stress states of the EF-induced migration of the collective skin epithelial cell, HaCaT. To investigate the state of cellular stresses in response to the EF, we first quantified local traction forces exerted by collective HaCaT monolayer using Fourier-transform traction microscopy (Trepat *et al.*, 2009). In both the pre- and post-EF stimulation, cellular traction showed substantial spatial heterogeneity with dynamic fluctuations in the magnitude and direction, evidenced by a color change in the locations marked by dotted circles (Figure 4, c–f). T_x represents the x component of traction, which is the axis perpendicular to

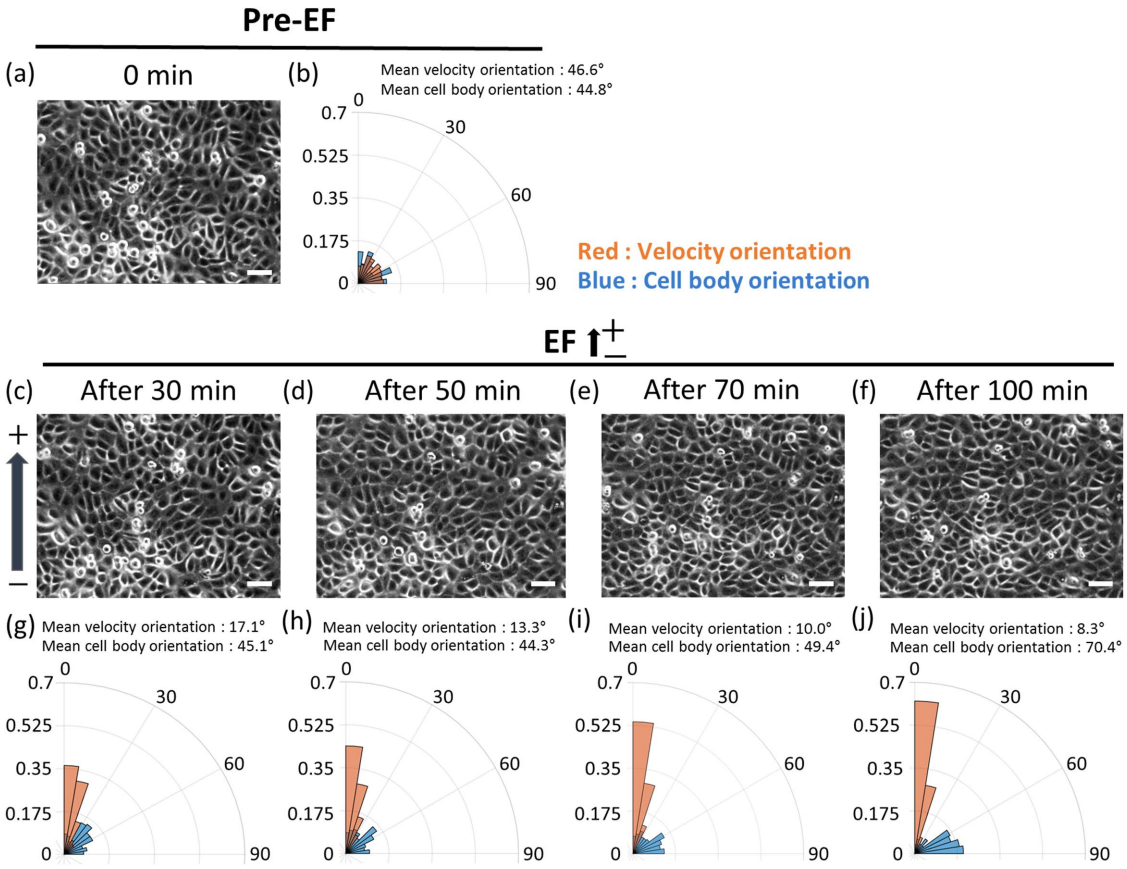

FIGURE 3: Perpendicular alignment of cell body follows the electrotactic migration. Phase contrast images of HaCaT monolayer under (a) pre-EF condition and (c–f) EF stimulation. Overlay of the angular distribution of cell velocity (red bars) and cell body (blue bars) at (b) pre-EF condition and (g–j) EF stimulation. (b) At the pre-EF condition, both cell velocity and cell body showed no preferred orientation. With the onset of EF stimulation, (g) cell velocity showed apparent alignment in the direction parallel to the EF within 30 min, while (h) the cell body still exhibited no biased alignment until 50 min. (i) After 70 min, the cell body showed the tendency of reorientation in the direction perpendicular to the EF, and (j) after 100 min, the cell body now showed apparent alignment in the direction perpendicular to the EF. Scale bars, 50 μm.

EF direction in our experimental setting (Figure 4, c and d), where the red indicates upward traction exerted on the substrate by the cells and the blue indicates downward traction exerted on the substrate by the cells. T_y represents the *y* component of traction, the axis parallel to EF direction (Figure 4, e and f; the red indicates rightward traction, and the blue indicates leftward traction). When the average magnitudes of the traction components were plotted as a function of time, we noticed a gradual, persistent decrease in the parallel component of traction with respect to the field direction ($|T_y|$, the red line in Figure 4g). However, the average traction magnitude perpendicular to the EF direction ($|T_x|$, the blue line in Figure 4g) showed negligible change. Thus, the $|T_x|/|T_y|$ ratio (gray line in Figure 4g) exhibited significant, steady increase for first 50 min after the onset of the EF stimulation. Fifty minutes of EF stimulation was shown to be insufficient for the completion of cell-body orientation.

Next, local intercellular stresses exerted among neighboring cells were calculated using the monolayer stress microscopy (MSM) technique (Tambe *et al.*, 2011, 2013). The MSM method encompasses the principle that the local tractions must be balanced by the intra- and intercellular forces according to Newton's laws. This method rests on the assumption that the cell monolayer behaves as a continuous, linear elastic material with Young's modulus *E* and Poisson's ratio ν. Young's modulus *E* is not relevant to the MSM solution, but Poisson's ratio ν can induce the inexact solution. Nevertheless, the effect of Poisson's ratio has been shown to be quite small; therefore, the solution recovers a wide range of the cell monolayer property (Tambe *et al.*, 2011, 2013). Recently, to exclude the effect of the cell monolayer rheology, an alternative method to measure stresses has been suggested (Nier *et al.*, 2016). On the basis of the previous report by Li *et al.* (2012) on the role of EF on intercellular junctions, we hypothesized that the intercellular stress should play a crucial role in the electrotactic response of the epithelial monolayer. To validate this, we utilized the MSM to visualize the intercellular stresses within the monolayer in both pre- and post-EF stimulation. The average normal intercellular stress of the HaCaT monolayer before the EF stimulation was tensile throughout the monolayer (compressive normal stress would have negative values) with the heterogeneous spatial distributions with varying magnitudes (Figure 5a). With the onset of EF, the overall magnitude of the average intercellular stress slightly increased while the spatial heterogeneity was still maintained (Figure 5, b–d, gray line in q). Since the EF contains the directional information, scalar value of intercellular stress alone would be insufficient to describe the physical stresses. We decomposed the local intercellular stress into *x*-*y* components where σ_{xx}

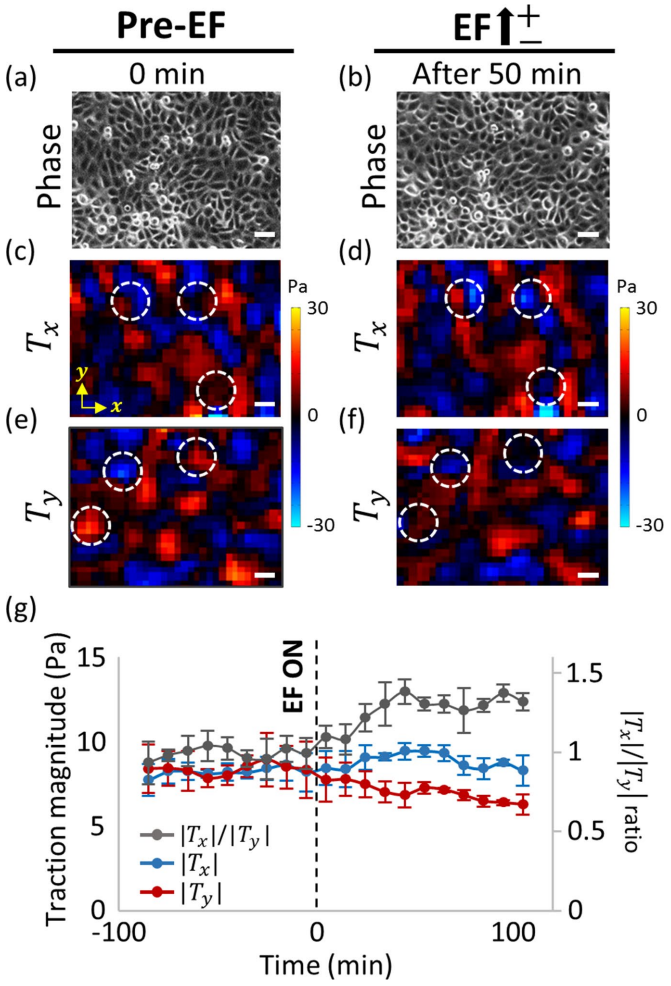

FIGURE 4: EF induces a polarized change of cellular traction force. (a, b) Phase contrast images, (c, d) maps of x component of traction (perpendicular to EF direction), and (e, f) the *y* component of traction (parallel to EF direction) at (a, c, e) pre-EF condition and (b, d, f) EF stimulating condition. White dotted circles indicate the locations of dynamic traction fluctuations in direction and magnitude. (g) Time evolution graph of the average magnitude of T_x (blue line) and T_y (red line) and the ratio of magnitude between T_x and T_y (gray line). Data are presented in 10-min intervals. Dashed line indicates the timepoint of EF initiation. Data are presented as mean ± SD ($n = 3$ independent monolayers). Scale bars, 50 μm.

corresponds to the stress tensor perpendicular to the EF direction and σ_{yy} corresponds to the stress tensor parallel to the EF direction. Before the EF stimulation, σ_{xx} and σ_{yy} were similar in magnitude (Figure 5, e and i, blue and red line in q). After the onset of EF, however, σ_{xx} increased dramatically (Figure 5, f–h, blue line in q) while σ_{yy} was only slightly affected (Figure 5, i–l, red line in q). This prominent increase in perpendicular stress tensor indicates the accumulation of tensile stress in tangential direction against the collective migration in the EF direction. In particular, the time period of 0–50 min was when the cells are migrating without reorientation of the cell body. The sudden drop in σ_{xx} at 80 min may correlate with the loosening of intercellular tension as cells were allowed to reorient in their ultimately preferred direction. We further investigated the intercellular stress anisotropy using the stress ellipse (Figure 5, m–p). The major axis of each ellipse indicates the maximum principal stress, and the minor axis indicates the minimum principal stress. The circularity of each ellipse indicates the degree of intercellular stress anisotropy, and the orientation of each ellipse shows the local principal stress orientation. Each ellipse was color coded to represent the degree of ellipse orientation departure from the *y*-axis, which is the axis representing the EF direction. Before EF stimulation, the orientation of ellipse distributed in all directions between 0° and 90° over the monolayer. Application of EF stimulation induced remarkable reorientation of intercellular stress toward the *x*-axis perpendicular to the EF direction (90° from the *y*-axis, red colored ellipse in Figure 5, n–p).

Physical stress reorientation precedes cell-body reorientation

From the observation of anisotropic change in the intercellular stress, we then asked which of the stress rearrangement and cell-body orientation comes first. To answer this question, we compared the time-course rearrangement of cell migration velocity, cell-body orientation, and intercellular stress orientation simultaneously by overlapping all data on the rose plots at pre-EF, 30 min, and 100 min after EF stimulation, respectively (Figure 5, s–u). At the pre-EF condition, all of the cell migration (red bars), cell body (blue bars), and intercellular stress (yellow bars) randomly oriented without any particular directedness (Figure 5s). Velocity field started to align in the direction parallel to the EF direction as early as 10 min after the onset of EF stimulation and aligned almost fully by the 25-min time point. However, intercellular stress exhibited no significant alignment until 20 min after the onset of EF and gradually aligned in the direction perpendicular to the EF direction (Figure 5r). After 30 min from the onset of the EF, nearly 70% of overall intercellular stress showed the considerable reorientation toward the perpendicular axis with respect to the EF direction, distributed between 60° and 90° from the EF direction. Between the migration velocity and intercellular stress, there existed lagging of stress behind the migration. However, cell-body orientation did not exhibit any preferred direction within 30 min (Figure 5t). At 100 min from the onset of EF stimulation, the cell migration was mostly synchronized along the EF direction, and the intercellular stress dominantly well aligned perpendicular to the EF direction. At this time point, cell body now showed significantly biased orientation aligned with the intercellular stress (perpendicular to the EF direction) (Figure 5u). Our results confirmed that cell-body orientation happened at last, following rapid electrotactic migration response and then physical stress alignment in the monolayer. Reorientation of intercellular tensile stress in the direction perpendicular to the EF must correlate closely with intracellular cytoskeletal rearrangement, leading to the cell-body orientation in the same direction.

Reversed EF redirects migration of collective monolayer without rearrangement of intercellular stress

During the abrupt change in the EF direction, cells in isolation could change direction by either reversing their polarity or by making a smooth U-turn in space in the absence of the physical constraints from neighboring cells or obstacles (Allen *et al.*, 2013). What would happen if the EF direction were reversed in a monolayer of cells tightly held together by intercellular tension? A recent study by Cohen *et al.* (2014) reported evidence that showed the local collective "U-turn" redirection in an MDCK cell monolayer.

To clarify the physical basis for the redirection mechanism of the monolayer, we analyzed the intercellular stress orientation during the reversal of the EF. In our experiment, the monolayer was shown to migrate upward in a synchronized manner under the continued exposure to EF for 100 min, the anode being on top of the page (Figure 6a). After a sudden reversal of the EF by exchanging the

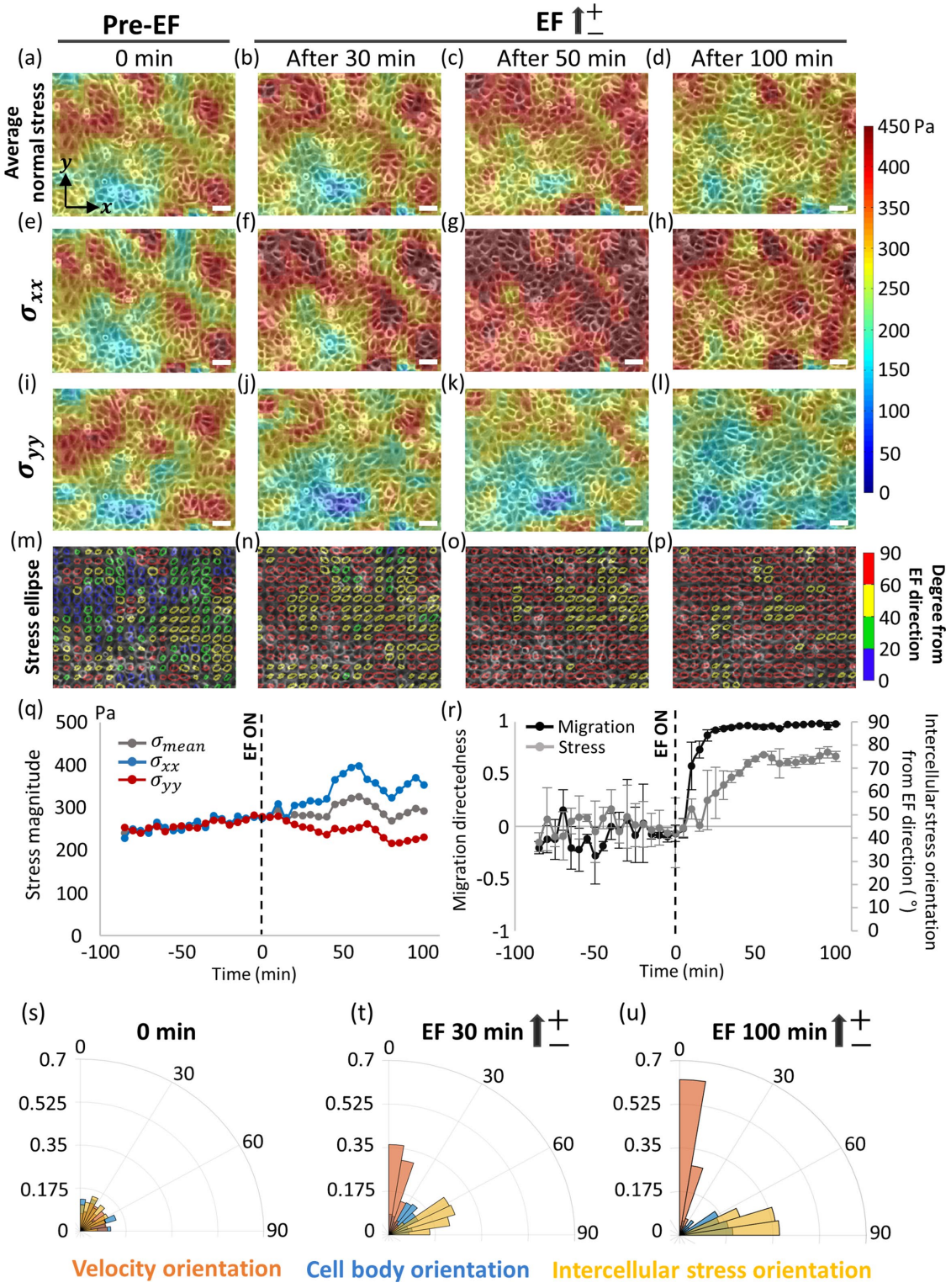

FIGURE 5: EF induces polarized intercellular stress that precedes the cell-body alignment. Maps of (a–d) average normal intercellular stress), (e–h) σ_{xx} (stress component perpendicular to the EF direction), and (i–l) σ_{yy} (stress component parallel to the EF direction) overlaid on phase contrast images at pre-EF and EF stimulating condition. With EF, σ_{xx} largely increased while σ_{yy} slightly decreased. (m–p) Color-coded stress ellipses overlaid on phase contrast images at pre-EF and EF stimulating condition. Color-code indicates the orientation of stress ellipse from the EF direction. (q) Time evolution graph of intercellular stress magnitude in 5-min time intervals. The ray line shows average normal intercellular stress, the blue line shows σ_{xx}, and the red line shows σ_{yy}. Lines indicate mean value ($n = 3$ independent monolayers). (r) Time evolution graphs of migration directedness (black line) and stress orientation (gray line) in 5-min intervals. Degree indicates departure of stress orientation from the *y*-axis (direction of EF). 0° indicates parallel direction to EF and 90° indicates perpendicular direction to EF. Data are presented as mean ± SD ($n = 3$ independent monolayers). Migration started to align already from 10 min after EF start and dominantly aligned around 25 min after EF stimulation. However,

anode and the cathode, HaCaT cells underwent a transient change in their migration behavior (Figure 6b) and finally synchronized themselves to migrate toward the new anode (Figure 6c). During the transient repolarization of migration, the upward directedness of migration diminished while either rightward or leftward movements were observed for a short duration (Figure 6e). This orthogonal migration with respect to the EF orientation spatiotemporally emerged as cooperative packs consisted of ~10 cells, displaying patches of swirl-like patterns within the monolayer. As shown in Figure 6, d–g, tracking the displacement of centroids of two selected cells showed the local "U-turn" reorientation over the course of ~60 min. This U-turn behavior has also been reported by Cohen *et al*. (2014) in the MDCK monolayer. Time-course measurement of average migration directedness confirmed the approximately ~60-min time delay between the EF reversal and actual cellular redirection response (Figure 6n). This time delay consisted of three phases. First, for ~20 min after the EF reversal, the monolayer persisted in the directional migration induced by the initial EF stimulation. Between 20 and 40 min, the migration directedness was randomly oriented and, finally, by the 60-min time point, it rapidly recovered in the reversed direction toward the new anode. During the dynamic alteration in migration, the average normal intercellular stress showed insignificant change in magnitude (Figure 6, h–j). Consistently, as evidenced by the stress ellipse, the stress orientation was maintained without any transient changes throughout the entire redirection process of migration once the intercellular stress aligned perpendicular to the EF field (Figure 6, k–m and o). Cell-body orientation also maintained its perpendicular orientation to the EF direction during the redistribution of the velocity profile (Figure 6, p–r). These data suggest that the intercellular stress state within the monolayer is maintained during the EF-driven U-turn migration of the HaCaT monolayer.

DISCUSSION

The EF is a strong guidance cue that can override other coexisting guidance cues from microenvironment (Zhao *et al.,* 2009). Thus, the endogenous EF is expected to play a key role in essential physiological events such as tissue regeneration and development by inducing the directional response of the cells. Especially, during the wound healing of skin tissues, a sheet migration of epithelial monolayer during the reepithelization process is known to be driven by endogenous EF. While the importance of such collective response to EF has been well accepted, the underlying physical mechanism is yet to be elucidated. In this study, development of the integrated platform to simultaneously stimulate dcEF while observing cells and measuring cellular tractions enabled us to investigate the time evolution of collective electrotactic response of a monolayer.

Since the discovery of EF-directed cell migration in the late 19th century, extensive studies investigated the role of EF in directing migration and cellular morphology across many cell types. In addition to the phenomenological observation of electrotactic cellular response, researchers investigated the mechanism of how the EF was sensed by the cells. A number of studies identified the cellular membrane as the primary sensor for the EF (Huang *et al.,* 2009; Minc and Chang, 2010; Allen *et al.,* 2013; Sun *et al.,* 2013). EF-induced asymmetry in the membrane characteristics was believed to be delivered through the polarized biochemical signaling pathways, ultimately regulating the migratory machinery inside the cell to direct the migration. For a migratory response, the change in cellular traction and cytoskeletal rearrangements would be expected. Indeed, when a single cell was stimulated by EF, the immediate change in the cellular traction was observed followed by the morphological rearrangement (Curtze *et al.,* 2004). Li *et al*. visualized the cellular traction force of the EF-stimulated epithelial monolayer using the deflection of underlying microposts (Li *et al*., 2012), and the discontinuous distribution of microposts was unsuitable for the calculation of the intercellular stresses among neighboring cells. Polyacrylamide gel as the continuous underlying substrate for traction measurement was beneficial to quantify the EF-induced changes in cellular tractions and their correlations with the intimate neighbors within the collective monolayer.

Using the MSM method, Tambe *et al*. (2011) observed the coincidence of the local direction of migration and the local orientation of maximal principal stress in collective cell migration and defined this phenomenon as "plithotaxis." While the plithotaxis is physically intuitive and consistent with the tension-induced polarization of cellular migration, an exceptional case has been reported by Kim *et al*. (2013). When the advancing cell monolayer was forced to encounter the nonadhesive vacant space, the local velocity vectors veered systematically away from the orientations of the principal stress by angles approaching 90° (Kim *et al*., 2013). What we observed in our study with the EF is similar to what Kim *et al*. showed with the frustrated edge where both cases consistently show the perpendicular alignment of the orientation of principal stress and local velocity vectors rather than parallel one predicted by the plithotaxis.

Dynamic alterations in the physical stresses and the morphological reorientation during electrotactic responses shared some of the common characteristics with the case of the shear flow induced realignment of endothelial cell monolayer reported by Steward *et al.* (2015). Endothelial monolayer exhibited an early alignment of the traction forces and intercellular stresses along the direction of the shear flow followed by the delayed cell-body alignment. This evidence inferred that intercellular stress-guided morphological reorganization in the collective monolayer may be generalized to other situations of exogenously applied stimulators such as chemical gradient or cyclic stretch. However, we identified the clear distinctions between electrotactic- and shear flow-induced responses. Unlike the gradual attenuation of intercellular stress triggered by the shear flow on the endothelial monolayer (Steward *et al.,* 2015), the EF strengthened the intercellular stress and reoriented the principal axes of stress ellipse in the direction perpendicular to the EF as shown in Figure 5. The reversal of the EF had little effect on both the strength of the intercellular stresses and the orientation of the stress ellipse of the intercellular stresses (Figure 6).

intercellular stress started to have alignment tendency not until 20 min after EF start and gradually aligned perpendicularly from the EF direction until 50 min. (s–u) Overlay of angular distribution of cell velocity (red bars), cell body (blue bars), and intercellular stress (yellow bars). (s) At pre-EF condition, velocity, body, and stress showed no preferred alignment. (t) After 30 min from the EF initiation, dominant population of velocity already well oriented parallel to the EF direction. Intercellular stress also showed considerable reorientation to perpendicular axis to the EF direction. Cell body, however, showed no preferred orientation. (u) At 100 min after EF stimulation, velocity and intercellular stress were even better aligned parallel and perpendicular to the EF direction, respectively. Now the cell body aligned perpendicular to the EF direction (90°) with relatively weak tendency. Dashed lines indicate the EF initiation. Scale bars, 50 μm.

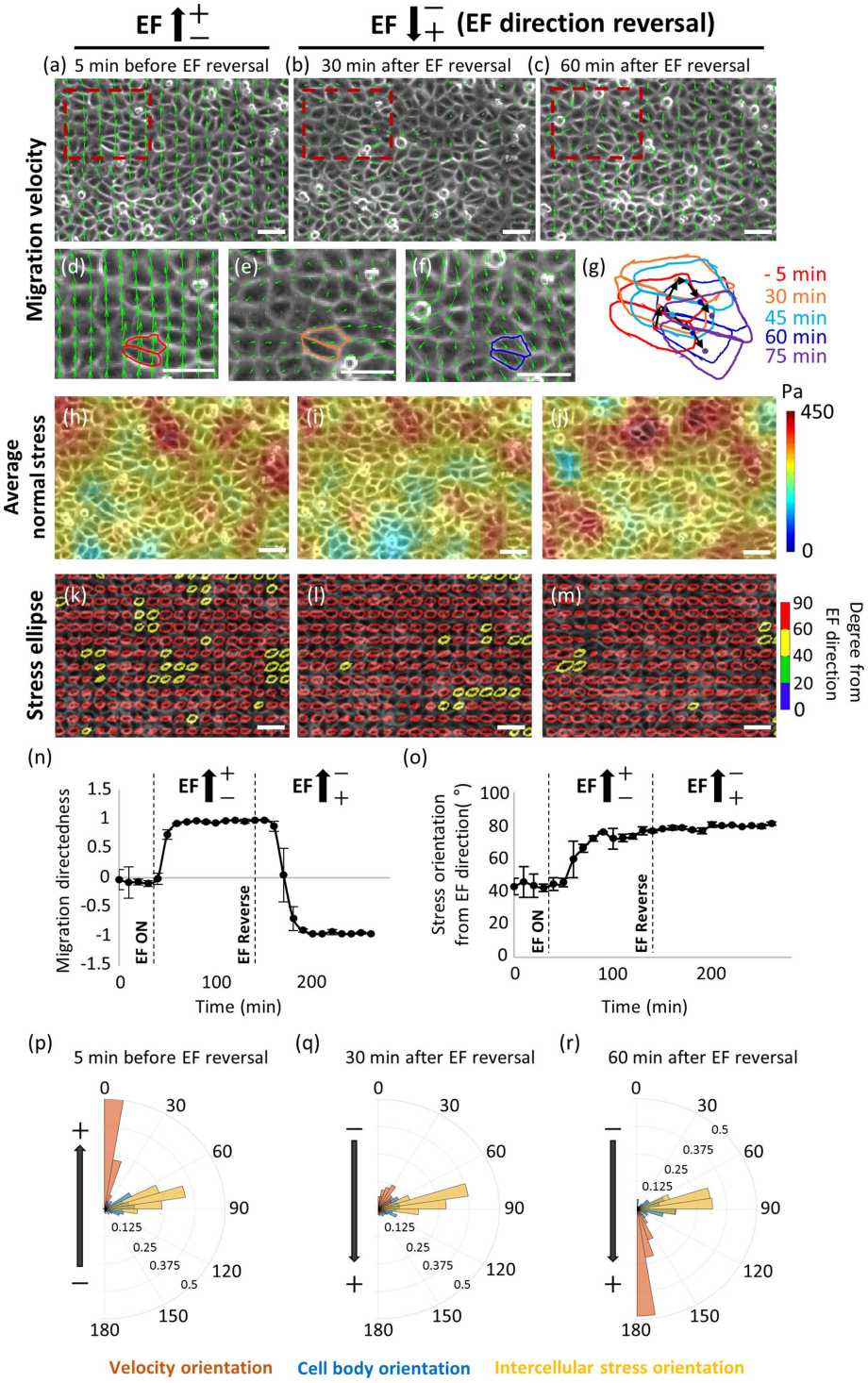

FIGURE 6: Maintenance of intercellular stress during the EF-induced reversal of collective migration. (a–c) Redirection process of HaCaT monolayer induced by the reversal of EF direction. (d–f) Enlarged field of red dotted boxes in a–c. (g) Outlines of the representative cells in d–f showing the time-course relative positions. Dots represent the position of centroids at each time point. Black arrows represent the relative displacement of centroids. (h–j) Maps of average normal intercellular stress overlaid on phase contrast images. (k–m) Color-coded stress ellipses overlaid on phase-contrast images showed no transient change of stress alignment during the reversal of EF direction. (n) Time evolution graph of average migration directedness of the monolayer in 10-min intervals during the pre-EF, first EF stimulation with the anode on top, and sudden reversal of EF direction. (o) Time evolution graph of intercellular stress orientation in 10-min intervals. (p–r) Overlay of angular distribution of cell velocity (red bars), cell body (blue bars), and intercellular stress (yellow bars) during the reversal of EF direction. Data are presented as mean ± SD ($n = 3$ independent monolayers). Scale bars, 50 μm.

The adherens junction, where cadherins are anchored to the cytoskeletal structure through α- and β-catenin, mainly regulates the force transmission and accumulation between neighboring cells (Maître and Heisenberg, 2013). These adherens junctions exhibit plasticity, continually formed and disassembled, to maintain the epithelial characteristics (Baum and Georgiou, 2011). Therefore, the polarized intercellular stress-driven morphological alignment might originate from the polarized remodeling of the adherens junction complex along the cell–cell interface in the direction of the EF, inducing a stress ellipse in the direction orthogonal to the EF. In particular, given the importance of α-catenin in the HaCaT monolayer for the coordinated contraction, the anisotropic accumulation of α-catenin may be a promising candidate responsible for the EF-induced directional enhancement of intercellular stress (Vedula *et al.*, 2014, 2015).

In this study, we provided the evidence suggesting that the EF-induced intercellular stress reorientation drives the cell-body alignment while the electrotatic migration happens independently of the reorientation of either intercellular stress or cellular morphology. Once the intercellular stresses were aligned, the reversal of the EF direction induced the reversed migration of the cells without any apparent disruption of the intercellular stress, suggesting that the dislodging of the physical stress alignment along the adjacent cells not be necessary for changing the direction of monolayer migration. The reversal of EF also confirmed that the orthogonal arrangement of intercellular stress with respect to the EF direction is irrespective of the polarity of the EF. These observations imply that the anodal/cathodal exchange only directly influence the direction of migration, whereas the intercellular stress orientation is aligned perpendicular to the axis of EF itself rather than affected by the position of anodal/cathodal polarity.

MATERIALS AND METHODS

Cell culture

HaCaT cells, derived from spontaneously immortalized human keratinocytes, were cultured in DMEM supplemented with 10% FBS and 1% penicillin/streptomycin at 37°C with 5% CO_2.

EF stimulating chamber

The EF chamber consisted of three parts: the slide-glass base part, the first PDMS layer, and the second PDMS layer (Figure 1). First, the slide-glass base part (76 × 52 mm, height of 1.3 mm; Matsunami) was cleaned with ethanol. For the curved chamber geometry,

the first PDMS layer was prepared by patterning the desired geometry on a 1 mm height of the PDMS sheet. Then both slide-glass base part and the first PDMS layer were O_2 plasma-treated for the permanent bonding. After the attached parts were autoclaved and sterilized, PA gel (Young's modulus = 3 kPa, thickness = 100 μm) was fabricated on the surface of the linear chamber geometry, where becomes the cell observation area. Gel preparation followed the protocols reported in previous publications (Butler *et al.*, 2002; Kandow *et al.*, 2007). For the stable bonding between the glass and PA gel, the surface of the slide glass was treated with silane. During the gel polymerization, we mixed fluorescent beads (diameter = 0.5 μm; FluoSpheres; Life Technologies) in the gel, loaded a 24-μl drop of PA gel on the base part, and immediately centrifuged the attached base part to pull up every bead to the surface of the PA gel. For the cell attachment on the gel, the PA gel surface was functionalized with sulfosuccinimidyl-6-(4-azido-2-nitrophenylamino) hexanoate (Sulfo-SANPAH; Proteochem) and 1 mg/ml in 50 mM HEPES buffer (Life Technologies) and coated with 10 μg/ml collagen type I (PureCol; Advanced BioMatrix). After HaCaT cell monolayer was seeded on the PA gel (details described below), the 6-mm height of the second PDMS layer was finally covered on the first PDMS layer to form the channel at the observation region, and media were filled in the chamber. The assembled chamber was mounted on the microscope, and agar bridges were placed into each media reservoir. The other ends of agar bridges were connected to the voltage-controlled power source via Ag/AgCl electrodes in beakers filled with 5x Steinberg's solution (Figure 1). The field strength at the cell observation window was measured at the beginning and end of the experiment through Ag/AgCl monitoring electrodes placed at both ends of the enclosed chamber by voltage meter.

Cell monolayer seeding

To seed the HaCaT cells in the observation region of the chamber, we prepared 10:1 PDMS stencil with rounded rectangular patterns and covered it on the gel substrate. Before seeding the cells, patterns in the stencil were carefully filled with DMEM to avoid the generation of air bubbles. Next, a 200-μl drop of cell suspension with 1×10^6 cells/ml density was loaded into the PDMS stencil. After allowing cells to settle down and attach to the substrate for ~1 h, the remaining cells were flushed out by gentle pipetting. Then the cells were incubated for additional 12 h to form a confluent monolayer with mature cell–cell junctions. Immediately before mounting the chamber on the microscope, the PDMS stencil was carefully removed, and the second PDMS layer was placed to seal the observation region.

Region of interest

During the assembly of the EF stimulation system, we remove the PDMS stencil to prevent the undesirable distortion of the EF. Once the stencil was removed, cells at the edge were free to move outward with active lamellipodia while the cells in the core, far enough away from the edge, exhibited distinct phenotypes (Poujade *et al.*, 2007). In this study, we aimed to focus on the effect of EF only within the bulk of the confluent monolayer. For this reason, we eliminated any potential edge effects by confining our region of interest only within the interior location of the monolayer, at least 12–15 rows of the cells (250 μm) from the nearest free edge.

Time-lapse imaging

Phase-contrast and fluorescence bead images of the cell monolayer within the region of interest were taken every 5 min using the 5× objective lens. All experiments were performed on the Axiovert 200M (Carl Zeiss) microscope with the maintenance of incubating condition (37°C and 5% CO_2).

PIV analysis

Acquired stack images of the experiment were stabilized using either ImageJ or MATLAB. Postprocessed images were then analyzed by custom particle image velocimetry (PIV) software written in MATLAB for the measurement of the velocity field. We used cross-correlation with a window size of 64×64 pixels allowing spatial resolution of 16 μm.

Cell migration velocity and directedness

Cell migration calculated by PIV analysis from 5-min interval images was analyzed to determine the migration velocity and directedness. Cell migration velocity indicates the instantaneous velocity quantified from the displacement of the cell between two successive images at every time points. Directedness indicates the directional information of migration shown as $\cos\theta$, where θ represents the angle between the axis parallel to EF direction and the cell migration direction. Therefore, if the average cell direction was parallel to the EF, with the average value of θ close to 0° or 180°, directedness was close to 1(upward migration) or –1(downward migration). Average value of directedness close to 0 represented the random migration.

Quantification of cell-body orientation

Cell-body orientation was quantified by the angle between the long axis of the cell and the axis parallel to the EF direction. The long axis of the cell was defined as the major axis of the ellipsoidal fit of the cell boundary. All of these steps were conducted using ImageJ (Supplemental Figure S1).

Fourier transform traction microscopy

Traction maps exerted by the cell monolayer were measured from the bead displacements in the gel using the unconstrained Fourier transform traction microscopy, which was well described in previously published references (Butler *et al.*, 2002; Trepat *et al.*, 2009).

Monolayer stress microscopy

To calculate the intercellular stress, we used the monolayer stress microscopy (MSM) reported by Tambe *et al.* (2011, 2013). MSM calculated intercellular stress based on the measured traction by applying straightforward force balance according to Newton's law; the two-dimensional stress tensor within the monolayer must be balanced by the traction. At each point within the monolayer, the stress tensor perpendicular to the EF direction (σ_{xx}) and parallel to the EF direction (σ_{yy}) were presented in data. To obtain the principal stresses, $\sigma_{max,}$ and σ_{min}, the coordinate was converted at each point within the monolayer by eigenvalue decomposition. From the principal stresses, the local average normal stress was defined as $(\sigma_{max} + \sigma_{min})/2$, which represents the scalar tension within the monolayer. To represent the intercellular stress orientation, we plotted stress ellipse with the σ_{max} at the major axis and the σ_{min} at the minor axis. The local principal stress orientation defined the local stress orientation, represented by the ellipse orientation in this report (Kim *et al.*, 2013; Steward *et al.*, 2015).

ACKNOWLEDGMENTS

The Matlab codes for TFM and MSM were generously provided by J. J. Fredberg's lab at the Harvard T. H. Chan School of Public Health. This work was supported by National Research Foundation of Korea (NRF) grants funded by the Korean Government (NRF-2013S1A2A2035518, NRF-2015M3A9B3028685, and NRF-2016K2A9A2A08003761).

REFERENCES

Allen GM, Mogilner A, Therlot JA (2013). Electrophoresis of cellular membrane components creates the directional cue guiding keratocyte galvanotaxis. Curr Biol 23, 560–568.

Baum B, Georgiou M (2011). Dynamics of adherens junctions in epithelial establishment, maintenance, and remodeling. J Cell Biol 192, 907–917.

Butler JP, Tolić-Nørrelykke IM, Fabry B, Fredberg JJ (2002). Traction fields, moments, and strain energy that cells exert on their surroundings. Am J Physiol Cell Physiol 282, 595–605.

Cohen DJ, Nelson WJ, Maharbiz MM (2014). Galvanotactic control of collective cell migration in epithelial monolayers. Nat Mater 13, 409–417.

Cooper MS, Keller RE (1984). Perpendicula orientation and directional migration of amphibian neural crest cells in dc electrical fields. Proc Natl Acad Sci USA 81, 160–164.

Cooper MS, Schliwa M (1985). Electrical and ionic controls of tissue cell locomotion in DC electric fields. J Neurosci Res 13, 223–244.

Cortese B, Palama IE, D'Amone S, Gigli G (2014). Influence of electrotaxis on cell behavior. Integr Biol 6, 817–830.

Curtze S, Dembo M, Miron M, Jones DB (2004). Dynamic changes in traction forces with DC electric field in osteoblast-like cells. J Cell Sci 117, 2721–2729.

Fang KS, Ionides E, Oster G, Nuccitelli R, Isseroff RR (1999). Epidermal growth factor receptor relocalization and kinase activity are necessary for directional migration of keratinocytes in DC electric fields. J Cell Sci 112, 1967–1978.

Funk RHW (2015). Endogeneous electric fields as guiding cue for cell migration. Front Physiol 6, 143.

Gomez GA, McLachlan RW, Yap AS (2011). Productive tension: force-sensing and homeostasis of cell-cell junctions. Trends Cell Biol 21, 499–505.

Harris AK, Pryer NK, Paydarfar D (1990). Effects of electric fields on fibroblast contractility and cytoskeleton. J Exp Zool 253, 163–176.

Huang L, Cormie P, Messerli MA, Robinson KR (2009). The involvement of Ca2+ and integrins in directional responses of zebrafish keratocytes to electric fields. J Cell Physiol 219, 162–172.

Jang H, Notbohm J, Gweon B, Cho Y, Park CY, Kee SH, Fredberg JJ, Shin JH, Park Y (2017). Homogenizing cellular tension by hepatocyte growth factor in expanding epithelial monolayer. Sci Rep 7, 45844.

Kandow CE, Georges PC, Janmey PA, Beningo KA (2007). Polyacrylamide hydrogels for cell mechanics: steps toward optimization and alternative uses. Methods Cell Biol 83, 29–46.

Kim JH, Serra-Picamal X, Tambe DT, Zhou EH, Park CY, Sadati M, Park JA, Krishnan R, Gweon B, Millet E, *et al.* (2013). Propulsion and navigation within the advancing monolayer sheet. Nat Mater 12, 856–863.

le Duc Q, Shi Q, Blonk I, Sonnenberg A, Wang N, Leckband D, de Rooij J (2010). Vinculin potentiates E-cadherin mechanosensing and is recruited to actin-anchored sites within adherens junctions in a myosin II-dependent manner. J Cell Biol 189, 1107–1115.

Li L, Hartley R, Reiss B, Sun Y, Pu J, Wu D, Lin F, Hoang T, Yamada S, Jiang J, Zhao M (2012). E-cadherin plays an essential role in collective directional migration of large epithelial sheets. Cell Mol Life Sci 69, 2779–2789.

Luther PW, Peng HB (1983). Changes in cell shape and actin distribution induced by constant electric fields. Nature 303, 61–64.

Maître JL, Heisenberg CP (2013). Three functions of cadherins in cell adhesion. Curr Biol 23, 626–633.

Maruthamuthu V, Sabass B, Schwarz US, Gardel ML (2011). Cell-ECM traction force modulates endogenous tension at cell-cell contacts. Proc Natl Acad Sci USA 108, 4708–4713.

McCaig CD, Rajnicek AM, Song B, Zhao M (2004). Controlling cell behavior electrically: current views and future potential. Physiol Rev 85, 943–978.

McCaig CD, Zhao M (1997). Physiological electrical fields modify cell behavior. BioEssays 19, 819–826.

Minc N, Chang F (2010). Electrical control of cell polarization in the fission yeast Schizosaccharomyces pombe. Curr Biol 20, 710–716.

Mycielska ME, Djamgoz MBA (2004). Cellular mechanisms of direct-current electric field effects: galvanotaxis and metastatic disease. J Cell Sci 117, 1631–1639.

Nakajima K, Zhu K, Sun Y, Hegyi B, Zeng Q, Murphy CJ, Small JV, Chen-Izu Y, Izumiya Y, Penninger JM, Zhao M (2015). KCNJ15/Kir4.2 couples with polyamines to sense weak extracellular electric fields in galvanotaxis. Nat Commun 6, 8532.

Nier V, Jain S, Lim CT, Ishihara S, Ladoux B, Marcq P (2016). Inference of internal stress in a cell monolayer. Biophys J 110, 1625–1635.

Poujade M, Grasland-Mongrain E, Hertzog A, Jouanneau J, Chavrier P, Ladoux B, Buguin A, Silberzan P (2007). Collective migration of an epithelial monolayer in response to a model wound. Proc Natl Acad Sci USA 104, 15988–15993.

Pu J, McCaig CD, Cao L, Zhao Z, Segall JE, Zhao M (2007). EGF receptor signaling is essential for electric-field-directed migration of breast cancer cells. J Cell Sci 120, 3395–3403.

Pu J, Zhao M (2004). Golgi polarization in a strong electric field. J Cell Sci 118, 1117–1128.

Robinson KR (1985). The responses of cells to electrical fields: a review. J Cell Biol 101, 2023–2027.

Song B, Gu Y, Pu J, Reid B, Zhao Z, Zhao M (2007). Application of direct current electric fields to cells and tissues *in vitro* and modulation of wound electric field *in vivo*. Nat Protoc 2, 1479–1489.

Song B, Zhao M, Forrester JV, McCaig CD (2002). Electrical cues regulate the orientation and frequency of cell division and the rate of wound healing *in vivo*. Proc Natl Acad Sci USA 99, 13577–13582.

Steward RJR, Tambe D, Hardin CC, Krishnan R, Fredberg JJ (2015). Fluid shear, intercellular stress, and endothelial cell alignment. Am J Physiol Cell Physiol 308, 657–664.

Sun Y, Do H, Gao J, Zhao R, Zhao M, Mogilner A (2013). Keratocyte fragments and cells utilize competing pathways to move in opposite directions in an electric field. Curr Biol 23, 569–574.

Tambe DT, Croutelle U, Trepat X, Park CY, Kim JH, Millet E, Butler JP, Fredberg JJ (2013). Monolayer stress microscopy: limitations, artifacts and accuracy of recovered intercellular stresses. PLoS One 8, e55172.

Tambe DT, Hardin CC, Angelini TE, Rajendran K, Park CY, Serra-picamal X, Zhou EH, Zaman MH, Butler JP, Weitz DA, *et al.* (2011). Collective cell guidance by cooperative intercellular forces. Nat Mater 10, 469–475.

Trepat X, Wasserman MR, Angelini TE, Millet E, Weitz DA, Butler JP, Fredberg JJ (2009). Physical forces during collective cell migration. Nat Phys 5, 426–430.

Vasioukhin V, Bauer C, Yin M, Fuchs E (2000). Directed actin polymerization is the driving force for epithelial cell-cell adhesion. Cell 100, 209–219.

Vedula SRK, Hirata H, Nai MH, Brugués A, Toyama Y, Trepat X, Lim CT, Ladoux B (2014). Epithelial bridges maintain tissue integrity during collective cell migration. Nat Mater 13, 87–96.

Vedula SRK, Peyret G, Cheddabi I, Chen T, Brugues A, Hirata H, Lopez-Menendez H, Toyama Y, Almeida LN, Trepat X, *et al.* (2015). Mechanics of epithelial closure over non-adherent environments. Nat Commun 6, 6111.

Zhao M (2009). Electrical fields in wound healing—an overriding signal that directs cell migration. Semin Cell Dev Biol 20, 674–682.

Zhao M, Agius-Fernandez A, Forrester JV, McCaig CD (1996). Orientation and directed migration of cultured corneal epithelial cells in small electric fields are serum dependent. J Cell Sci 109, 1405–1414.

Zhao M, Bai H, Wang E, Forrester JV, McCaig CD (2003). Electrical stimulation directly induces pre-angiogenic responses in vascular endothelial cells by signaling through VEGF receptors. J Cell Sci 117, 397–405.

Zhao M, Dick A, Forrester JV, McCaig CD (1999). Electric field directed cell motility involves upregulated expression and asymmetric redistribution of the EGF receptors and is enhanced by fibronectin and lamin. Mol Biol Cell 10, 1259–1276.

Zhao M, Pu J, Forrester JV, McCaig CD (2002). Membrane lipids, EGF receptors, and intracellular signals colocalize and are polarized in epithelial cells moving directionally in a physiological electric field. FASEB J 16, 857–859.

Zhao M, Song B, Pu J, Wada T, Reid B, Tai G, Wang F, Guo A, Walczysko P, Gu Y, *et al.* (2006). Electrical signals control wound healing through phosphatidylinositol-3-OH kinase-γ and PTEN. Nature 442, 457–460.